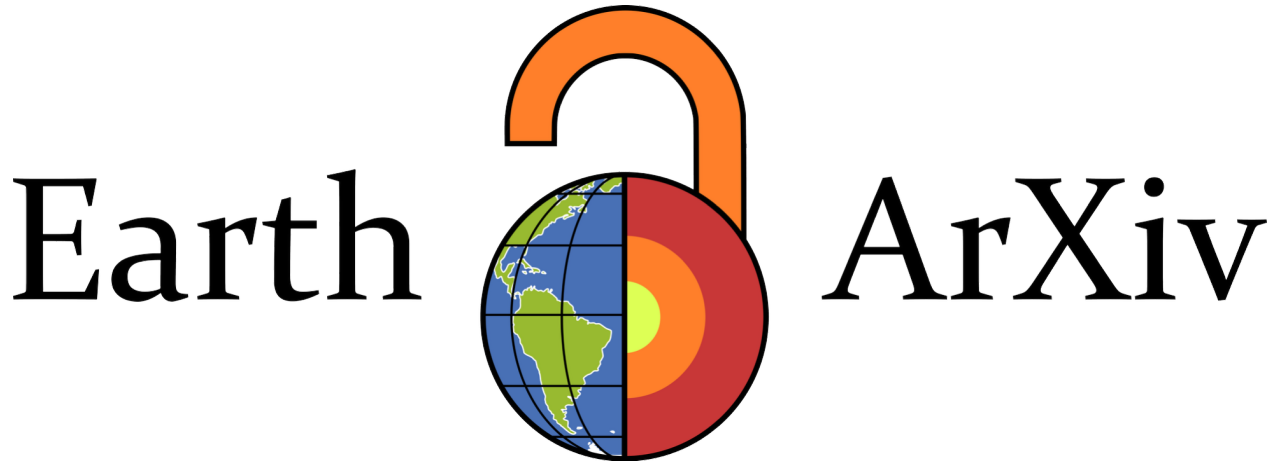

Sudden freshening and cooling of western North Atlantic slope water at the onset of the Little Ice Age based on Magnesium-to-Calcium ratio and oxygen stable isotope record.

Wai Ching Rachel Chu[1,2], Tiffany Audet[3], Anne de Vernal[3], Benoit Thibodeau[1,*]

[1]Department of Earth and Environmental Sciences & School of Life Sciences, The Chinese University of Hong Kong, Sha Tin, N.T., Hong Kong S.A.R, China.

[2]Now at School of Ocean and Earth Science, Faculty of Environmental and Life Science, University of Southampton, Southampton, SO17 1BJ, United Kingdom.

[3]GEOTOP, Université du Québec à Montréal, Montréal, Québec, Canada.

Corresponding author:

*Benoit Thibodeau; Email address: benoit.thibodeau@cuhk.edu.hk

ABSTRACT

The Little Ice Age (LIA), a period from ~1400 CE to 1850 CE, was characterized by colder winters and more frequent extreme weather events, particularly in the Northern Hemisphere. While the exact causes of the LIA remain a topic of ongoing research, evidence suggests that changes in ocean circulation likely contributed to the observed global cooling, although the specific mechanisms and drivers of these changes are not yet fully understood. Here, we aim to generate new knowledge to help us better understand how ocean circulation changed before, during, and after this climatic event. More specifically, using marine cores collected at the head of the Laurentian Channel in the Lower Estuary of the St. Lawrence, we investigated variations in the temperature and seawater oxygen isotopic signal of western North Atlantic slope waters to assess the relative strength of the Labrador Current and the Gulf Stream. First, we established a Mg/Ca-temperature calibration curve for *Globobulimina auriculata* from the bottom water of the Lower St. Lawrence Estuary based on instrumental temperature data and geochemical analysis from a short, century-old sediment box core. Then, using a longer piston core, we produced new downcore measurements of Mg/Ca in *Globobulimina auriculata* for the LIA. We then coupled this new temperature reconstruction with existing oxygen isotope data ($d^{18}O_{calcite}$) to disentangle the influence of temperature on the $d^{18}O_{calcite}$. The resulting $d^{18}O_{seawater}$ record is interpreted in terms of changes in in their isotopic composition due to changes in freshwater input, and relative strength and position of the Labrador Current and the Gulf Stream. Our interpretation suggests dominance of fresh Labrador Sea-derived waters around 1500 CE, and during most of the LIA. In the later stage of the LIA, after 1800 CE, our data indicate a steep increase in the influence of Atlantic-derived waters, consistent with a northward shift of the Gulf Stream. The record of the ~1800-1950 CE interval exhibits high-amplitude variability, with a sudden freshening event at the end of the LIA. The upper part of the record, after 1950 CE, is characterized by a

regional warming trend that has been widely documented in previous studies conducted in this area.

Keywords

Mg/Ca ratio, foraminifera, oxygen isotope, St Lawrence Estuary, temperature reconstruction, Little Ice Age, Labrador Current, Gulf Stream, AMOC, Paleoceanography

INTRODUCTION

The Little Ice Age (LIA) is a relatively short climate anomaly (~1400-1850CE, with variable onset timing depending on the region), characterized by abrupt cooling and glacier expansion, following the warming in Medieval Climate Anomaly (MCA) (Brönnimann et al., 2019; Wanner et al., 2022). The LIA is the coldest period in the last 8,000 years, being 0.7 – 1°C cooler in the Northern Hemisphere than in the 2000 CE (Lean and Rind, 1999). It is also associated with a higher frequency of extreme weather and more extreme seasonal temperatures. Due to the higher land coverage, the Northern Hemisphere was suggested to be more affected than the Southern Hemisphere (Wanner et al., 2022). The socio-economic impacts of the LIA have been relatively well documented (e.g., Behringer 1999; Fan 2023; Putnam et al. 2016), making it a valuable period for understanding how abrupt climate change may affect our livelihoods. It also provides valuable insights into ocean-climate interactions. Its late occurrence provided us with relatively high resolution in the sedimentary records. While the dominating factors causing the onset of LIA are poorly understood, previous studies suggest that atmosphere-ocean feedback may have played a significant role (Moffa-Sánchez et al. 2019).

The Atlantic Meridional Overturning Circulation (AMOC) is a branch of the thermohaline circulation in the North Atlantic Ocean (Buckley and Marshall, 2016; Ferreira et al., 2010), The Gulf Stream and the Labrador Current are two of the main ocean currents constituting the overturning circulation. and they are also part of the North Atlantic subpolar gyre (Figure 1). The Gulf Stream is a northeastward-flowing warm surface current originating in the Gulf of Mexico, bringing heat up the meridians, while the Labrador Current is a cold surface current flowing southward along the North Atlantic coast under the Coriolis force. Their respective strengths have been used to assess changes in the AMOC strength across different intervals, such as the Holocene and modern times (Ezer, 2015; Rashid et al., 2017; Thibodeau et al., 2018, 2010). While the strength of the AMOC has experienced large amplitude variations during Earth's history, slight variations are often overlooked but may be as informative about the potential consequences of global warming for the AMOC (Galaasen et al., 2020; Thibodeau et al., 2025).

During the LIA, changes in the AMOC may have impacted meridional heat transport to higher latitudes, thereby influencing the climate of the North Atlantic and subpolar regions (Moffa-Sánchez et al. 2014). Multiple studies have attempted to characterize changes in AMOC and identify its drivers during this period (Table 1); two different mechanisms have been proposed to explain changes in AMOC, i.e., wind forcing and freshwater forcing. In the wind forcing scenario, the negative North Atlantic Oscillation caused weaker northwestern wind and more frequent Southern wind, leading to a weaker Labrador Current, which was also associated with a northward shift in the Gulf Stream (Jutras et al., 2023; Sicre et al., 2014), thus resulting in a weaker AMOC. On the other hand, in the freshwater forcing scenario, the increase in storminess (Dawson et al., 2007) during LIA led to more sea ice formation, break-off, and rafting, which eventually melted and contributed to the Labrador

Current. The large quantity of freshwater decreased the salinity, lowering the density gradient and thus weakening Labrador Sea convection and the subpolar gyre convection, resulting in a decreased AMOC (Alonso-Garcia et al., 2017; Holliday et al., 2020; Moffa-Sánchez et al., 2014; Moffa-Sánchez and Hall, 2017; Rashid et al., 2023; Thibodeau et al., 2018, 2010; Thornalley et al., 2018). While it is widely acknowledged that both mechanisms contributed to a potentially weaker AMOC, debates have focused on which forcing was more predominant (Moffa-Sánchez et al. 2014; Sicre et al. 2014), a question that could be resolved by determining the strength of the Labrador Current during the LIA. The freshwater hypothesis would support a stronger Labrador Current (Sicre et al. 2014; Rashid et al. 2023), whereas the wind stress hypothesis would imply that more freshwater flowed through the Fram Strait, thus strengthening the East Greenland Current and weakening the Labrador Current (Jutras et al., 2023).

Previous reconstructions of northwestern Atlantic oceanography have described a sharp cooling from the MCA to the LIA (Keigwin, 1996) and a progressive increase in the relative contribution of Atlantic-derived water in the Laurentian Channel toward the end of the LIA, as evidenced by oxygen isotope records from benthic foraminifera (Thibodeau et al. 2018). More recent work also suggested a gradual replacement of Labrador-derived water throughout the LIA based, again, on $\delta^{18}O_{calcite}$ measurements and end-member mixing calculations (Keigwin et al., 2025). However, disentangling the temperature and $\delta^{18}O_{seawater}$ solely from the $\delta^{18}O_{calcite}$ is complex and relies on a set of assumptions, notably the consistency of the endmembers over time. In this paper, we present new Mg/Ca data from benthic foraminifera as a temperature proxy to disentangle the contribution from changes in water masses in the oxygen isotope signal. We aim to provide new insights into

oceanographic changes in the NW Atlantic during the LIA and thus contribute to a better understanding of the relationship between AMOC, the subpolar gyre, and climate.

Magnesium-to-Calcium (Mg/Ca) ratio in carbonates is a commonly used paleothermometer with increasing popularity The Mg/Ca ratio in perforate foraminiferal tests is determined both biologically and by the chemical properties of ambient seawater (Bentov and Erez, 2006; Erez, 2003), and its strong dependence on temperature makes it a suitable paleothermometer. The temperature correlation can be deduced from biological (Bentov and Erez, 2006) and physical factors (Alkhatib et al., 2022; Katz, 1973; Mucci, 1987; Rosenthal et al., 1997). The solubility of calcite decreases with increasing temperature (Segnit et al., 1962), and more Mg^{2+} is incorporated into inorganically precipitated calcite with increasing temperature. Temperature also enhances ATP hydrolysis, the chemical process that converts ATP to ADP and releases energy. Since ATP molecules can bind free Mg^{2+} ions, enhanced ATP hydrolysis results in less ATP available and thus fewer Mg^{2+} ions to be bound by ATP. This process increases the concentration of free Mg^{2+} ions in the cellular environment, thus increasing the Mg/Ca ratio (Bentov and Erez, 2006; Romani and Maguire, 2002). Another factor governing the Mg/Ca ratio in calcite is the diffusion constant of Mg^{2+} ions, which increases with temperature, facilitating diffusion between ambient seawater and the vacuole of the foraminifers (Bentov and Erez, 2006).

In this paper, we used in-solution ICP-MS measurements from individual foraminifer test to establish a Mg/Ca-temperature calibration curve for *Globobulimina auriculata* in the lower St. Lawrence Estuary. By removing the temperature signal from oxygen isotopic data, we then reconstructed the relative proportions of Labrador Current and Atlantic water entering

154 the Laurentian Channel to better understand the dynamics of these water masses during the
155 LIA.
156
157 **METHODOLOGY**
158 **Sediment core and subsampling**

159 Two sediment cores obtained from the St. Lawrence Estuary were used for this study (Figure
160 S1). Core CR02-23 is a 0.12 m^2 x 0.5 m long and was collected at 48º42.008'N, 68º38.894'W
161 at 345m, during an expedition of the *R/V Coriolis II* in 2002 CE. The age-depth model of the
162 core was previously established using Pb-210 (Thibodeau et al., 2010, 2006). A 1.8-yr age
163 uncertainty was calculated in the age model (Figure S2). Five cm^3 of wet sediment was taken
164 at 1-cm intervals from 0 to 30 cm, with an additional sampling at 0.5 cm depth. The depth
165 corresponded to 1933 – 2001 CE. The average sediment rate was 0.42 cm/yr. Analyses of this
166 CR02-23 core were used to establish a Mg/Ca–temperature calibration equation.

167 Core MD99-2220 is 51.6 m long and was collected at 48°38.32N, 68°37.93W, at 320 m of
168 water depth during an expedition of the *R/V Marion Dufresne* in 1999. The upper 14 cm of
169 the core was missing due to handling disturbances (St-Onge et al., 2003). The
170 lithostratigraphy of the core had been divided into two units, Unit 1 from the base of the core
171 to 1497 cm), and Unit 2 from 1497 cm to the surface. Unit 1 consists of grey to dark grey
172 laminated to massive clays, while Unit 2 consists of postglacial bioturbated silty clay (St-
173 Onge et al., 2003). The age-depth model was established using radiocarbon dating (St-Onge
174 et al., 2003), with a 2σ uncertainty of ±100 yr. For our study of the LIA interval, 5 cm^3 of wet
175 sediment was taken from the core at 1-cm intervals from 0 cm to 75.5 cm, with an additional
176 sample at 0.5 cm depth. The study interval spans from 1396 to 1975 CE, which covers the
177 LIA (Figure S3). According to the age model of St-Onge et al. (2003), sedimentation rates are

approximately 0.74 cm/yr for the upper 20 cm, 0.28cm/yr from 20 to 30 cm, and 0.15 cm/yr from 30 to 75 cm.

For all sample, wet sediment was sieved through a 63-μm mesh sieve to remove silt and clay. In the coarse fraction, foraminifera were examined under the Leica EZ4W Stereomicroscope, and specimens of *Globobulimina auriculata* were identified and hand-picked. In most samples, four intact foraminifer shells were selected from each depth as replicates (Trejos et al., 2003).

Cleaning

The tests were cleaned according to the protocol of Barker et al. (2003), but without the reductive cleaning step to remove the Mn-oxide coatings (Martin and Lea, 2002). Previous study observed a 10-15% Mg/Ca ratio decrease after reductive cleaning (Barker et al., 2003; Martin and Lea, 2002). However, only a 0.03 mmol/mol (i.e., ~1%) decrease in Mg/Ca is expected if all Mn-Fe oxide coating is removed (Barker et al., 2003). Given that the Mg/Ca ratio in this foraminifer species is low, averaging 3.65 mmol/mol, we did not perform a reductive cleaning step to avoid excessive Mg/Ca loss.

Single-foraminifer ICP-MS Analysis

All measurements were performed using an Agilent 7900 ICP-MS at the Chinese University of Hong Kong. As an internal standard, we used JCp-1, a certified coral reference material developed by the Geological Survey of Japan, and utilized for other foraminiferal studies (e.g. Zhou et al., 2022; Yoshimura et al., 2011). A self-made multi-element solution (MeRC) served as a reference material, comprising a mixture of pure Ca, Mg, Sr, Mn, and Fe solutions and 2% nitric acid. The accuracy and precision (<5%) of MeRC were measured with ICP-MS. Each run of the ICP-MS analysis was composed of 2% nitric acid blank

203 acquisition at the start and end of the run. Every five foraminiferal sample acquisitions were
204 accompanied by a set of reference material and 2% nitric acid blank for recalibration and
205 brief cleaning of the machine. Details of the ICP-MS setup are reported in the supplementary
206 information.
207 Raw data were obtained from the ICP-MS Data Analysis window software (Agilent
208 Technologies, 2014). Because ICP-MS can be relatively unstable, frequent recalibration of
209 the instrument against reference materials is required (Jackson and Sylvester, 2008). Re-
210 calibration was done with MeRC correction, in which the cps of each elemental isotope in the
211 first MeRC acquisition of each run was used as the baseline. These baseline cps values were
212 then compared against the subsequent MeRC acquisitions within the same run. Variations
213 between MeRC acquisition and the baseline were computed to define the linear slope. The
214 samples in between acquisitions were corrected with the respective slope. To mitigate the
215 effects of omitting a reductive cleaning step, data exceeding the elimination thresholds
216 determined from our data and from literature were considered contaminated (see Table S2).
217
218 *CR02-23 Calibration Curve and Temperature Reconstruction Comparison*
219 The downcore comparison of MeRC-corrected $^{24}Mg/^{48}Ca$ data and instrumental temperature
220 compiled by Thibodeau et al. (2010), led to the establishment of our calibration curves, which
221 were compared with both linear fit and exponential fit. The $^{24}Mg/^{48}Ca$ data led to the
222 reconstruction of the bottom water temperature (*t in Celsius*), and were compared using the
223 following calibration equations :
224 1) Anand et al. (2003), who used paired Mg/Ca and $\delta^{18}O$ measurements in 11 planktic
225 foraminifera species:
226 $$Mg/Ca\ (mmol/mol) = (0.38 \pm 0.02)\ e^{((0.090 \pm 0.003)t)}$$

2) Lear et al. (2002), who used benthic foraminifera belonging to *Cibicidoides* from core-tops:

$$Mg/Ca\ (mmol/mol) = (0.867 \pm 0.049)\ e^{((0.109 \pm 0.007)t)}$$

3) Weldeab et al. (2016), who used the genus *Globobulimina*:

$$Mg/Ca\ (mmol/mol) = (0.36\ \pm 0.02)t + 2.22 \pm 0.19$$

Salinity Effect

The salinity impact on the Mg/Ca ratio in foraminifera is under debate, especially for benthic foraminifera (e.g. Mathien-Blard and Bassinot 2009; Weldeab, Arce, and Kasten 2016). To investigate the effect of salinity on our Mg/Ca data, two approaches were used. 1) Mg/Ca data were analysed against the instrumental salinity data at 300 m depth in the study area (Galbraith et al., 2018); 2). Differences between our Mg/Ca data and back-calculated Mg/Ca from the Weldeab et al. (2016) equation in *Globobulimina* (see above) were compared to instrumental salinity:

MD99-2220 Parent Water Mass Reconstruction

The calibration curve from the core CR02-23 Mg/Ca data was applied to reconstruct bottom-water temperature from core MD99-2220. Using the $\delta^{18}O_{(calcite)}$ data previously obtained for MD99-2220 (Thibodeau et al., 2018), we could calculate the $\delta^{18}O_{(seawater)}$ signal from the equation of Marchitto et al. (2014), which assumes a 0.9‰ offset for vital effect as measured for *Globobulimina affinis* (Hoogakker et al., 2010):

$$t\ (^{o}\ C) = \frac{0.245 - \sqrt{0.045461 + 0.0044(\ \delta^{18}O\ _{(calcite)} - \delta^{18}O\ _{(seawater)})}}{0.0022}$$

Given that the Atlantic Temperate Slope Water (ATSW) and Labrador Sea Slope Water (LSSW) have distinct $\delta^{18}O$ signals, we can track the change of contribution from $\delta^{18}O_{(seawater)}$ changes (Thibodeau et al. 2018, 2010). In the $\delta^{18}O_{(seawater)}$ reconstruction, a positive signature represents a dominant ATSW (proxy for Gulf Stream) and a negative signature represents a dominant LSSW (proxy for Labrador Current). A 95% confidence interval was applied for all statistical analyses, and all results were corrected to two decimal places, apart from cps, R-squares, and equations. All analyses and graphs were produced on GraphPad Prism 9.0 and Excel, while maps were produced via the use of Ocean Data View.

RESULT

CR02-23

In core CR02-23, measurements were made in a total of 75 samples of foraminifera. All elemental isotopes measured exceeded the limits of detection (LOD) and quantification (LOQ), indicating quantifiable concentrations.

Mg/Ca Ratio

After applying the elimination threshold (Table S2), 43 measurements remained for analysis. The $^{24}Mg/^{48}Ca$ ranges from 1.72 to 9.01 mmol/mol (Table S3). The p-value for the linear regression model of isotope ratios was < 0.05, representing a significant relationship between bottom water temperature and Mg/Ca ratio (Figure 2a). For both linear and non-linear (exponential) models, the R-squared values were > 0.7, indicating a significant correlation between temperature and the Mg/Ca ratio (Table S4). The exponential equation is chosen because it yielded a higher R-squared ($R^2=0.76$) than that of the linear model ($R^2=0.74$).

Salinity Effect and Contamination

No statistically significant relationship was observed between salinity and Mg/Ca (p-value >0.05, R-square>0.02; Figure 2b and Table S5). However, the lack of correlation could result from the small sample size (n=8) and the narrow salinity range (32.34 to 34.94 psu). No significant correlation was observed between Mn/Ca or Fe/Ca with Mg/Ca (Figure 3). A low but significant correlation was observed between Al/Ca and Mg/Ca, suggesting minimal contamination.

MD99-2220

A total of 286 foraminiferal samples were analysed. After applying the elimination threshold, 100 measurements remained for data analysis.

The average Mg/Ca ratio in MD99-2220 across depths 0 cm to 76 cm ranged from 1.14 to 9.16 mmol/mol. Reconstruction yielded bottom-water temperatures of 1.58-7.18°C (Figure 4a). We observed a stepwise increase in temperature from ~1396 to 1905 CE, followed by a decrease from ~1905 CE onwards.

The seawater isotope signal declined from the base of the record until ~1500 CE, then increased stepwise until ~1870 CE, after which a sharp decrease was recorded (Figure 4b). Because of the relatively high standard deviation of our measurements, we remained cautious when discussing small-amplitude variations in our record.

DISCUSSION

Calibration of Mg/Ca vs temperature in the St. Lawrence Estuary

Comparisons of Calibrations

We compared the CR02-23 Mg/Ca ratio with previously established calibrations for

299 temperature estimates from Mg/Ca, thereby testing the applicability of published equations
300 (Anand et al., 2003; Lear et al., 2002; Weldeab et al., 2016) for *G. auriculata* at our study
301 location. The temperature reconstructions using published equations yield a wide range of
302 values (-1 to 28 °C), well outside the study environment's range (3 to 6 °C). This highlights
303 the need for a regional calibration curve using *Globobulimina auriculata.*
304
305 *Calibration Equation for* Globobulimina auriculata *in the Lower St. Lawrence Estuary*
306 The calibration equation was established as the best-fit exponential equation from $^{24}Mg/^{48}Ca$
307 data after MeRC correction and instrumental temperature from the St. Lawrence bottom
308 water (Thibodeau et al., 2018):
309 $$Mg/Ca\ (mmol/mol) = 0.6341e^{(0.3740t)}$$
310 *where t represents water temperature in Celsius*
311
312 This equation yielded a range of bottom-water temperatures of 3.0 to 5.5°C, with an R-square
313 of 0.76 between instrumental and estimated values.
314
315 It is important to note that this calibration used Mg/Ca values from the sediment core and
316 instrumental temperature records on a calendar-year scale. Therefore, the correlation may be
317 affected by uncertainty in the core chronology. Moreover, because we used the local
318 temperature gradient over time, the calibration covers only a 3 °C temperature range. While
319 this calibration can provide a fine-scale reconstruction, the narrow temperature range may
320 have amplified uncertainty in the relationship between the actual and reconstructed data,
321 resulting in a relatively low coefficient of correlation. Finally, assuming that carbonate ion
322 concentration mainly affects the Mg/Ca ratio at bottom-water temperatures < 3 °C (Elderfield
323 et al. 2006), we did not account for the effect of carbonate ion, which may be an additional

caveat. Regardless of these potential limitations, the calibration equation tailored to *Globobulimina auriculata* in the Lower St. Lawrence Estuary appears robust for regional reconstructions of temperature through time.

Little Ice Age temperature reconstruction

Changes in bottom-water temperature reconstructed from our Mg/Ca data followed a pattern similar to that of the parent water masses, the Labrador Current and Atlantic Water, as indicated by the change in calculated $\delta^{18}O_{seawater}$ (Figure 4b). Since different temperatures characterize the two water masses, the dominant factor controlling temperature changes is likely related to the mixing proportions of parent water masses in the bottom water of the lower St. Lawrence Estuary.

The non-parametric Mann-Kendall Trend Test was applied to identify significant trends. A positive trend characterized the 1490 to 1850 CE interval for both $\delta^{18}O_{seawater}$ and temperature (Table S6). Transitions were thus identified at 1490 and 1850 CE, yielding three time intervals in the study sequence (Figure 5), which are discussed hereafter with reference to potential drivers of change in the dynamics of western North Atlantic circulation during the LIA.

Transition from MCA to LIA (~1400 to ~1490 CE)

This time interval was characterized by a relatively constant signal, followed by a relatively sharp decrease in both temperature and oxygen isotope in the latter half of the 15th century. Before the onset of the LIA, a significant stratospheric sulphur loading from explosive volcanic activity, in conjunction with reduced solar irradiance during the Spörer minimum, may have contributed to a general climate cooling (Lean and Rind, 1999; Miller et al., 2012).

These events occurred immediately before the drastic change in parent water mass/oxygen isotope observed in our record between ~1470 and 1500. The combined effect of volcanism and low solar irradiance caused a short-lived cooling (Miller et al., 2012) and extreme weather events (Brönnimann et al., 2019). Increasing storminess recorded in the GISP2 ice core around ~1400 CE (Dawson et al. 2007; Mayewski et al., 1997; Trouet et al., 2012), which was later interpreted as an increase in intensity of storms during LIA (Knudsen et al., 2014). Extreme weather conditions may have led to enhanced fractioning of sea ice due to strong winds. The broken sea ice then melted and could have entered the Labrador Current through the Canadian Archipelago Route as freshwater. In addition, Arctic meltwater during the warm Medieval Climate Anomaly (MCA) could increase the freshwater supply to the Labrador Current (Moffa-Sánchez et al., 2014; Lapointe and Bradley, 2021). High meltwater and freshwater discharge could potentially explain the strengthening of the surface and subsurface Labrador Current and colder waters, as estimated at ~1350 CE from TEX_{86}-T and higher presence of Polar waters at Eirik Drift (Rashid et al., 2023), relatively cool condition in the Sargasso Sea (Keigwin, 1996) and relatively low $\delta^{18}O$, indicating fresh and cold condition, in the Jordan Basin (Keigwin et al., 2025). This cooling was synchronous with an increase in the size of sortable silt from Southeast Grand Banks, suggesting an increase in Labrador Current flow speed since ~1450 CE, before the rise in the contribution of LSSW as reconstructed herein. Our data suggest a cooling of the bottom water from ~1470 CE (Figure 4), which is consistent with stronger Labrador Sea current-derived input.

The concurrent reduction in solar irradiance from extreme volcanism and solar minima may have caused general climate cooling and reduced northward heat transport, thereby shifting the Gulf Stream southward (Lund et al., 2006) and reducing the relative contribution of the ATSW as estimated from our record (Figure 4). Such reduced northward heat transport is

coincident with the decrease in the temperature-based AMOC index (Figure 5), likely due, at least in part, to the weakening of the ATSW branch.

Taken together, the external forcing, including increased volcanism and reduced solar insolation, may have indirectly led to the observed increase in the contribution of LSSW in the bottom waters of the St. Lawrence Estuary and a decrease in the contribution of ATSW, through high-latitude cold and freshwater input and reduced heat transport, respectively.

The Little Ice Age (~1500 to 1850 CE)

In the study region, the LIA was characterized by a significant increasing trend of oxygen isotope signature and bottom water temperature (Table S6). The coldest and freshest subsurface water in the Labrador Sea was recorded around 1580 CE, as indicated by Mg/Ca ratios and $\delta^{18}O$ values in *Neogloboquadrina pachyderma* (Thornalley et al., 2018). Additionally, a pulse of cold and fresh subsurface water was detected around 1620 CE based on $\delta^{18}O$ in *Turborotalita quinqueloba* (Moffa-Sánchez et al. 2014). Therefore, low bottom water temperature and strong contribution of LSSW at the start of LIA can be interpreted as the result of fresher than usual Labrador-derived water and a weak contribution from ATSW.

More saline waters of the Gulf Stream were reported around 1750 CE and attributed to drier conditions in a negative phase of the North Atlantic Oscillation (NAO) (Lund et al., 2006; Saenger et al., 2009). The increased salinity of the Gulf Stream, resulting in a higher oxygen isotope composition of the ATSW, might have contributed to the rise in $\delta^{18}O_{seawater}$ in our reconstruction (Figure 4b). Moreover, a negative NAO likely led to weaker NW winds and more frequent southerly winds (Sicre et al., 2014). With changes in wind stress, the weaker NW winds transport less sea ice along the Canadian Archipelago Route (West of Greenland). This, in turn, may lead to a decrease in the strength of the Labrador Current, which is

consistent with increased southward flow through the Fram Strait (Perner et al. 2011), where the high abundance of agglutinated Arctic water species at ~1650 CE was used as an indicator of increasing water flow through the Fram Strait. Therefore, a decreased influence from the Labrador Current throughout LIA may have led to higher temperature and oxygen isotope signals. This is consistent with other studies suggesting a gradual northward displacement of the Gulf Stream in the later stage of the LIA (Forman et al., 2025).

The end of LIA (~1810-1870 CE) coincides with the early stage of the industrial era (~1830 CE onwards), during which air temperature and sea surface temperature recorded a <0.2 °C and <0.5 °C increase, respectively (Abram et al., 2016). However, climate-related warming cannot account for the ~2 °C increase in bottom water temperature. Therefore, we hypothesize that the regional warming was mainly caused by the enhanced contribution of ATSW relative to LSSW. The timing of the peak matched the end of the large-scale ice-rafting events in ~1800 CE (Alonso-Garcia et al., 2017), the end of the series of volcanic eruptions (~1835 CE) (Brönnimann et al., 2019) and the northmost position of the Gulf stream (Forman et al., 2025). A decrease in the deep western boundary current (DWBC) was also inferred from sortable silt (Thornalley et al., 2018), which explains the maximum oxygen isotopic signal observed during this interval.

Post-LIA (~1871 CE onward)

The start of this interval was marked by a sharp decrease of approximately 2°C in estimated bottom-water temperature, suggesting a significant change in the parent water mass contribution, followed by a similar warming of approximately 2°C in the second half of the 20th century (Figure 4a). Interestingly, the observed cooling coincides with a short-lived peak in hematite-stained grain abundance in the Labrador Sea, indicating a sudden and significant

increase in Arctic sea-ice export through the Eastern Greenland Current (Alonso-Garcia et al., 2017). Therefore, the drop in $\delta^{18}O_{seawater}$ may be caused by an increase in Labrador-derived water, but also by the freshening of this endmember. Moreover, while the Gulf Stream was strengthening as well after the end of the LIA, its $\delta^{18}O_{seawater}$ also dropped by about ~0.3‰ (Lund et al., 2006). Therefore, evidence of lower $\delta^{18}O_{seawater}$ value in both endmembers composing the Laurentian bottom water suggests that the isotopic signal was primarily controlled by changes in the isotopic composition of these water masses due to freshwater input following the LIA. In the second half of the 20th century, we reconstructed a 2°C warming, coherent with multiple observations in the region and that was attributed to an increased influence of Atlantic-derived water over the Canadian shelf (Genovesi et al., 2011; Gilbert et al., 2005; Keigwin et al., 2025, 2003; Thibodeau et al., 2018, 2013, 2010, 2006).

CONCLUSION

In this paper, we used single foraminifer ICP-MS to establish an exponential Mg/Ca-temperature calibration curve for *Globobulimina auriculata* at the Lower St. Lawrence Estuary, i.e. $Mg/Ca\ (mmol/mol) = 0.6341e^{(0.3740t)}$. This bottom-water temperature reconstruction curve applies to a temperature range of 3.0-5.5°C. Despite its narrow temperature range, it provides a species- and region-specific curve for relatively accurate temperature reconstruction in future studies. Using the newly established calibration curve and Mg/Ca data from the MD99-2220 core, we reconstructed the bottom-water temperature in the Lower St. Lawrence Estuary during the LIA. Constrained by $\delta^{18}O_{calcite}$ data, we calculated the change in $\delta^{18}O_{seawater}$ and used it as a proxy for the change in the contribution of the parent water mass. Our results, taken together with previous evidence, indicate that the transition from MCA to LIA was characterized a sharp decrease in temperature and oxygen

isotope values, likely due to increased freshwater input. During the LIA, there was an increasing trend in oxygen isotope signal and bottom water temperature, with a shift from LSSW to ATSW dominance. The post-LIA period began with a sharp decrease in bottom water temperature, followed by a significant warming trend in the late 20th century, attributed to an increased influence of Atlantic-derived water masses over the Canadian continental shelf.

ACKNOWLEDGEMENT

This study was funded through the General Research Fund from the Research Grant Council of Hong Kong (#17301320) awarded to Benoit Thibodeau. The sampling and study of marine cores MD99-2220 and CR02-23 were enabled thanks to the support of the Natural Science and Engineering Research Council (NSERC) of Canada and the *Fonds de Recherche du Québec – Nature et Technologie* (FRQNT). The authors thank the technical support provided by Mr Cho On Thomas Tang from the Chinese University of Hong Kong for his help troubleshooting the Agilent 7900 ICP-MS.

DATA AVAILABILITY

Data will be available at https://doi.org/10.48668/HLKYYR upon acceptance of the paper.

REFERENCES

Abram, N.J., McGregor, H.V., Tierney, J.E., Evans, M.N., McKay, N.P., Kaufman, D.S., 2016. Early onset of industrial-era warming across the oceans and continents. Nature 536, 411–418. https://doi.org/10.1038/nature19082

Agilent Technologies, 2014. Agilent 7900 ICP-MS MassHunter Workstation User Guide.

Alkhatib, M., Qutob, M., Alkhatib, S., Eisenhauer, A., 2022. Influence of precipitation rate and temperature on the partitioning of magnesium and strontium in calcite overgrowths. Chemical Geology 599, 120841. https://doi.org/10.1016/j.chemgeo.2022.120841

Alonso-Garcia, M., Kleiven, H. (Kikki) F., McManus, J.F., Moffa-Sanchez, P., Broecker, W.S., Flower, B.P., 2017. Freshening of the Labrador Sea as a trigger for Little Ice Age development. Climate of the Past 13, 317–331. https://doi.org/10.5194/cp-13-317-2017

Anand, P., Elderfield, H., Conte, M.H., 2003. Calibration of Mg/Ca thermometry in planktonic foraminifera from a sediment trap time series. Paleoceanography 18. https://doi.org/10.1029/2002PA000846

Barker, S., Greaves, M., Elderfield, H., 2003. A study of cleaning procedures used for foraminiferal Mg/Ca paleothermometry. Geochemistry, Geophysics, Geosystems 4. https://doi.org/10.1029/2003GC000559

Behringer, W., 1999. Climatic Change and Witch-hunting: the Impact of the Little Ice Age on Mentalities. Climatic Change 43, 335–351. https://doi.org/10.1023/A:1005554519604

Bentov, S., Erez, J., 2006. Impact of biomineralization processes on the Mg content of foraminiferal shells: A biological perspective. Geochemistry, Geophysics, Geosystems 7. https://doi.org/10.1029/2005GC001015

Brönnimann, S., Franke, J., Nussbaumer, S.U., Zumbühl, H.J., Steiner, D., Trachsel, M., Hegerl, G.C., Schurer, A., Worni, M., Malik, A., Flückiger, J., Raible, C.C., 2019. Last phase of the Little Ice Age forced by volcanic eruptions. Nat. Geosci. 12, 650–656. https://doi.org/10.1038/s41561-019-0402-y

Bryan, S.P., Marchitto, T.M., 2008. Mg/Ca–temperature proxy in benthic foraminifera: New calibrations from the Florida Straits and a hypothesis regarding Mg/Li. Paleoceanography 23. https://doi.org/10.1029/2007PA001553

Buckley, M.W., Marshall, J., 2016. Observations, inferences, and mechanisms of the Atlantic Meridional Overturning Circulation: A review. Reviews of Geophysics 54, 5–63. https://doi.org/10.1002/2015RG000493

Dawson, A.G., Hickey, K., Mayewski, P.A., Nesje, A., 2007. Greenland (GISP2) ice core and historical indicators of complex North Atlantic climate changes during the fourteenth century: Holocene. Holocene 17, 427–434. https://doi.org/10.1177/0959683607077010

Elderfield, H., Yu, J., Anand, P., Kiefer, T., Nyland, B., 2006. Calibrations for benthic foraminiferal Mg/Ca paleothermometry and the carbonate ion hypothesis. Earth and Planetary Science Letters 250, 633–649. https://doi.org/10.1016/j.epsl.2006.07.041

Erez, J., 2003. The Source of Ions for Biomineralization in Foraminifera and Their Implications for Paleoceanographic Proxies. Reviews in Mineralogy and Geochemistry 54, 115–149. https://doi.org/10.2113/0540115

Ezer, T., 2015. Detecting changes in the transport of the Gulf Stream and the Atlantic overturning circulation from coastal sea level data: The extreme decline in 2009–2010 and estimated variations for 1935–2012. Global and Planetary Change 129, 23–36. https://doi.org/10.1016/j.gloplacha.2015.03.002

Fan, K., 2023. The Little Ice Age and the Fall of the Ming Dynasty: A Review. Climate 11, 71. https://doi.org/10.3390/cli11030071
Ferreira, D., Marshall, J., Campin, J.-M., 2010. Localization of Deep Water Formation: Role of Atmospheric Moisture Transport and Geometrical Constraints on Ocean Circulation. Journal of Climate 23, 1456–1476. https://doi.org/10.1175/2009JCLI3197.1
Forman, E.C.G., Baldini, J.U.L., Jamieson, R.A., Lechleitner, F.A., Walczak, I.W., Nita, D.C., Smith, S.R., Richards, D.A., Baldini, L.M., McIntyre, C., Müller, W., Peters, A.J., 2025. The Gulf Stream moved northward at the end of the Little Ice Age. Commun Earth Environ 6, 552. https://doi.org/10.1038/s43247-025-02446-3
Galaasen, E.V., Ninnemann, U.S., Kessler, A., Irvalı, N., Rosenthal, Y., Tjiputra, J., Bouttes, N., Roche, D.M., Kleiven, H. (Kikki) F., Hodell, D.A., 2020. Interglacial instability of North Atlantic Deep Water ventilation. Science 367, 1485–1489. https://doi.org/10.1126/science.aay6381
Galbraith, P.S., Chassé, J., Caverhill, C., Nicot, P., Gilbert, D., Lefaivre, D., Lafleur, C., n.d. Physical Oceanographic Conditions in the Gulf of St. Lawrence during 2017.
Genovesi, L., de Vernal, A., Thibodeau, B., Hillaire-Marcel, C., Mucci, A., Gilbert, D., 2011. Recent changes in bottom water oxygenation and temperature in the gulf of st. Lawrence: Micropaleontological and geochemical evidence. Limnology and Oceanography 56, 1319–1329. https://doi.org/10.4319/lo.2011.56.4.1319
Gilbert, D., Sundby, B., Gobeil, C., Mucci, A., Tremblay, G.H., 2005. A seventy-two-year record of diminishing deep-water oxygen in the St. Lawrence estuary: The northwest Atlantic connection. Limnology and Oceanography 50, 1654–1666. https://doi.org/10.4319/lo.2005.50.5.1654
Holliday, N.P., Bersch, M., Berx, B., Chafik, L., Cunningham, S., Florindo-López, C., Hátún, H., Johns, W., Josey, S.A., Larsen, K.M.H., Mulet, S., Oltmanns, M., Reverdin, G., Rossby, T., Thierry, V., Valdimarsson, H., Yashayaev, I., 2020. Ocean circulation causes the largest freshening event for 120 years in eastern subpolar North Atlantic. Nat Commun 11, 585. https://doi.org/10.1038/s41467-020-14474-y
Hoogakker, B., Elderfield, H., Oliver, K., Crowhurst, S., 2010. Benthic foraminiferal oxygen isotope offsets over the last glacial-interglacial cycle. Paleoceanography 25. https://doi.org/10.1029/2009PA001870
Jackson, S., Sylvester, P., 2008. Calibration strategies for elemental analysis. Signal 10, 100.
Jutras, M., Dufour, C.O., Mucci, A., Talbot, L.C., 2023. Large-scale control of the retroflection of the Labrador Current. Nat Commun 14, 2623. https://doi.org/10.1038/s41467-023-38321-y
Katz, A., 1973. The interaction of magnesium with calcite during crystal growth at 25–90°C and one atmosphere. Geochimica et Cosmochimica Acta 37, 1563–1586. https://doi.org/10.1016/0016-7037(73)90091-4
Keigwin, L.D., 1996. The Little Ice Age and Medieval Warm Period in the Sargasso Sea. Science 274, 1503–1508. https://doi.org/10.1126/science.274.5292.1503
Keigwin, L.D., Petrie, B., Boyle, E.A., 2025. Slope Water Intrusions Onto Canadian Atlantic Continental Shelf During the Past 1800 Years. Paleoceanography and Paleoclimatology 40, e2025PA005183. https://doi.org/10.1029/2025PA005183
Keigwin, L.D., Sachs, J.P., Rosenthal, Y., 2003. A 1600-year history of the Labrador Current off Nova Scotia. Climate Dynamics 21, 53–62. https://doi.org/10.1007/s00382-003-0316-6
Knudsen, M.F., Jacobsen, B.H., Seidenkrantz, M.-S., Olsen, J., 2014. Evidence for external forcing of the Atlantic Multidecadal Oscillation since termination of the Little Ice Age. Nat Commun 5, 3323. https://doi.org/10.1038/ncomms4323

Lapointe, F., Bradley, R.S., 2021. Little Ice Age abruptly triggered by intrusion of Atlantic waters into the Nordic Seas. Science Advances 7, eabi8230. https://doi.org/10.1126/sciadv.abi8230

Lea, D.W., Mashiotta, T.A., Spero, H.J., 1999. Controls on magnesium and strontium uptake in planktonic foraminifera determined by live culturing. Geochimica et Cosmochimica Acta 63, 2369–2379. https://doi.org/10.1016/S0016-7037(99)00197-0

Lean, J., Rind, D., 1999. Evaluating sun–climate relationships since the Little Ice Age. Journal of Atmospheric and Solar-Terrestrial Physics 61, 25–36. https://doi.org/10.1016/S1364-6826(98)00113-8

Lear, C.H., Rosenthal, Y., Slowey, N., 2002. Benthic foraminiferal Mg/Ca-paleothermometry: a revised core-top calibration. Geochimica et Cosmochimica Acta 66, 3375–3387. https://doi.org/10.1016/S0016-7037(02)00941-9

Lund, D.C., Lynch-Stieglitz, J., Curry, W.B., 2006. Gulf Stream density structure and transport during the past millennium. Nature 444, 601–604. https://doi.org/10.1038/nature05277

Martin, P.A., Lea, D.W., 2002. A simple evaluation of cleaning procedures on fossil benthic foraminiferal Mg/Ca. Geochemistry, Geophysics, Geosystems 3, 1–8. https://doi.org/10.1029/2001GC000280

Mathien-Blard, E., Bassinot, F., 2009. Salinity bias on the foraminifera Mg/Ca thermometry: Correction procedure and implications for past ocean hydrographic reconstructions. Geochemistry, Geophysics, Geosystems: G3 10. https://doi.org/10.1029/2008GC002353

Mayewski, P.A., Meeker, L.D., Twickler, M.S., Whitlow, S., Yang, Q., Lyons, W.B., Prentice, M., 1997. Major features and forcing of high-latitude northern hemisphere atmospheric circulation using a 110,000-year-long glaciochemical series. Journal of Geophysical Research: Oceans 102, 26345–26366. https://doi.org/10.1029/96JC03365

Miller, G.H., Geirsdóttir, Á., Zhong, Y., Larsen, D.J., Otto-Bliesner, B.L., Holland, M.M., Bailey, D.A., Refsnider, K.A., Lehman, S.J., Southon, J.R., Anderson, C., Björnsson, H., Thordarson, T., 2012. Abrupt onset of the Little Ice Age triggered by volcanism and sustained by sea-ice/ocean feedbacks. Geophysical Research Letters 39. https://doi.org/10.1029/2011GL050168

Moffa-Sánchez, P., Hall, I.R., 2017. North Atlantic variability and its links to European climate over the last 3000 years. Nat Commun 8, 1726. https://doi.org/10.1038/s41467-017-01884-8

Moffa-Sánchez, P., Hall, I.R., Barker, S., Thornalley, D.J.R., Yashayaev, I., 2014. Surface changes in the eastern Labrador Sea around the onset of the Little Ice Age. Paleoceanography 29, 160–175. https://doi.org/10.1002/2013PA002523

Moffa-Sánchez, P., Moreno-Chamarro, E., Reynolds, D.J., Ortega, P., Cunningham, L., Swingedouw, D., Amrhein, D.E., Halfar, J., Jonkers, L., Jungclaus, J.H., Perner, K., Wanamaker, A., Yeager, S., 2019. Variability in the Northern North Atlantic and Arctic Oceans Across the Last Two Millennia: A Review. Paleoceanography and Paleoclimatology 34, 1399–1436. https://doi.org/10.1029/2018PA003508

Mucci, A., 1987. Influence of temperature on the composition of magnesian calcite overgrowths precipitated from seawater. Geochimica et Cosmochimica Acta 51, 1977–1984. https://doi.org/10.1016/0016-7037(87)90186-4

Perner, K., Moros, M., Lloyd, J.M., Kuijpers, A., Telford, R.J., Harff, J., 2011. Centennial scale benthic foraminiferal record of late Holocene oceanographic variability in Disko Bugt, West Greenland. Quaternary Science Reviews 30, 2815–2826. https://doi.org/10.1016/j.quascirev.2011.06.018

Putnam, A.E., Putnam, D.E., Andreu-Hayles, L., Cook, E.R., Palmer, J.G., Clark, E.H., Wang, C., Chen, F., Denton, G.H., Boyle, D.P., Bassett, S.D., Birkel, S.D., Martin-Fernandez, J., Hajdas, I., Southon, J., Garner, C.B., Cheng, H., Broecker, W.S., 2016. Little Ice Age wetting of interior Asian deserts and the rise of the Mongol Empire. Quaternary Science Reviews 131, 33–50. https://doi.org/10.1016/j.quascirev.2015.10.033

Rashid, H., Piper, D.J.W., Lazar, K.B., McDonald, K., Saint-Ange, F., 2017. The Holocene Labrador Current: Changing linkages to atmospheric and oceanographic forcing factors. Paleoceanography 32, 498–510. https://doi.org/10.1002/2016PA003051

Rashid, H., Zhang, Z., Piper, D.J.W., Patro, R., Xu, Y., 2023. Impact of Medieval Climate Anomaly and Little Ice Age on the Labrador Current flow speed and the AMOC reconstructed by the sediment dynamics and biomarker proxies. Palaeogeography, Palaeoclimatology, Palaeoecology 111558. https://doi.org/10.1016/j.palaeo.2023.111558

Romani, A.M.P., Maguire, M.E., 2002. Hormonal regulation of Mg2+ transport and homeostasis in eukaryotic cells. Biometals 15, 271–283. https://doi.org/10.1023/a:1016082900838

Rosenthal, Y., Boyle, E.A., Slowey, N., 1997. Temperature control on the incorporation of magnesium, strontium, fluorine, and cadmium into benthic foraminiferal shells from Little Bahama Bank: Prospects for thermocline paleoceanography. Geochimica et Cosmochimica Acta 61, 3633–3643. https://doi.org/10.1016/S0016-7037(97)00181-6

Saenger, C., Chang, P., Ji, L., Oppo, D.W., Cohen, A.L., 2009. Tropical Atlantic climate response to low-latitude and extratropical sea-surface temperature: A Little Ice Age perspective. Geophysical Research Letters 36. https://doi.org/10.1029/2009GL038677

Segnit, E.R., Holland, H.D., Biscardi, C.J., 1962. The solubility of calcite in aqueous solutions—I The solubility of calcite in water between 75° and 200° at CO2 pressures up to 60 atm. Geochimica et Cosmochimica Acta 26, 1301–1331. https://doi.org/10.1016/0016-7037(62)90057-1

Sicre, M.-A., Weckström, K., Seidenkrantz, M.-S., Kuijpers, A., Benetti, M., Masse, G., Ezat, U., Schmidt, S., Bouloubassi, I., Olsen, J., Khodri, M., Mignot, J., 2014. Labrador current variability over the last 2000 years. Earth and Planetary Science Letters 400, 26–32. https://doi.org/10.1016/j.epsl.2014.05.016

St-Onge, G., Stoner, J.S., Hillaire-Marcel, C., 2003. Holocene paleomagnetic records from the St. Lawrence Estuary, eastern Canada: centennial- to millennial-scale geomagnetic modulation of cosmogenic isotopes. Earth and Planetary Science Letters 209, 113–130. https://doi.org/10.1016/S0012-821X(03)00079-7

Thibodeau, B., de Vernal, A., Hillaire-Marcel, C., Mucci, A., 2010. Twentieth century warming in deep waters of the Gulf of St. Lawrence: A unique feature of the last millennium. Geophysical Research Letters 37. https://doi.org/10.1029/2010GL044771

Thibodeau, B., de Vernal, A., Limoges, A., 2013. Low oxygen events in the laurentian channel during the holocene. Marine Geology 346, 183–191. https://doi.org/10.1016/j.margeo.2013.08.004

Thibodeau, B., de Vernal, A., Mucci, A., 2006. Recent eutrophication and consequent hypoxia in the bottom waters of the Lower St. Lawrence Estuary: Micropaleontological and geochemical evidence. Marine Geology 231, 37–50. https://doi.org/10.1016/j.margeo.2006.05.010

Thibodeau, B., Doherty, J.M., Alonso-García, M., Band, S., González-Lanchas, A., Not, C., Ren, H., 2025. Upper Ocean Instability in the Subpolar North Atlantic and Its Implications for Deep Water Formation During Interglacials. Paleoceanography and Paleoclimatology 40, e2024PA004935. https://doi.org/10.1029/2024PA004935

Thibodeau, B., Not, C., Zhu, J., Schmittner, A., Noone, D., Tabor, C., Zhang, J., Liu, Z., 2018. Last Century Warming Over the Canadian Atlantic Shelves Linked to Weak Atlantic Meridional Overturning Circulation. Geophys. Res. Lett. 45, 12,376-12,385. https://doi.org/10.1029/2018GL080083

Thornalley, D.J.R., Oppo, D.W., Ortega, P., Robson, J.I., Brierley, C.M., Davis, R., Hall, I.R., Moffa-Sanchez, P., Rose, N.L., Spooner, P.T., Yashayaev, I., Keigwin, L.D., 2018. Anomalously weak Labrador Sea convection and Atlantic overturning during the past 150 years. Nature 556, 227–230. https://doi.org/10.1038/s41586-018-0007-4

Trejos, T., Montero, S., Almirall, J.R., 2003. Analysis and comparison of glass fragments by laser ablation inductively coupled plasma mass spectrometry (LA-ICP-MS) and ICP-MS. Anal Bioanal Chem 376, 1255–1264. https://doi.org/10.1007/s00216-003-1968-0

Trouet, V., Scourse, J.D., Raible, C.C., 2012. North Atlantic storminess and Atlantic Meridional Overturning Circulation during the last Millennium: Reconciling contradictory proxy records of NAO variability. Global and Planetary Change, Perspectives on Climate in Medieval Time 84–85, 48–55. https://doi.org/10.1016/j.gloplacha.2011.10.003

Wanner, H., Pfister, C., Neukom, R., 2022. The variable European Little Ice Age. Quaternary Science Reviews 287, 107531. https://doi.org/10.1016/j.quascirev.2022.107531

Weldeab, S., Arce, A., Kasten, S., 2016. Mg/Ca-ΔCO3porewater2−–temperature calibration for Globobulimina spp.: A sensitive paleothermometer for deep-sea temperature reconstruction. Earth and Planetary Science Letters 438, 95–102. https://doi.org/10.1016/j.epsl.2016.01.009

Yoshimura, T., Tanimizu, M., Inoue, M., Suzuki, A., Iwasaki, N., Kawahata, H., 2011. Mg isotope fractionation in biogenic carbonates of deep-sea coral, benthic foraminifera, and hermatypic coral. Anal Bioanal Chem 401, 2755–2769. https://doi.org/10.1007/s00216-011-5264-0

Zhou, X., Hess, A.V., Bu, K., Sagawa, T., Rosenthal, Y., 2022. Simultaneous Determination of I/Ca and Other Elemental Ratios in Foraminifera: Comparing Results From Acidic and Basic Solutions. Geochemistry, Geophysics, Geosystems 23, e2022GC010660. https://doi.org/10.1029/2022GC010660

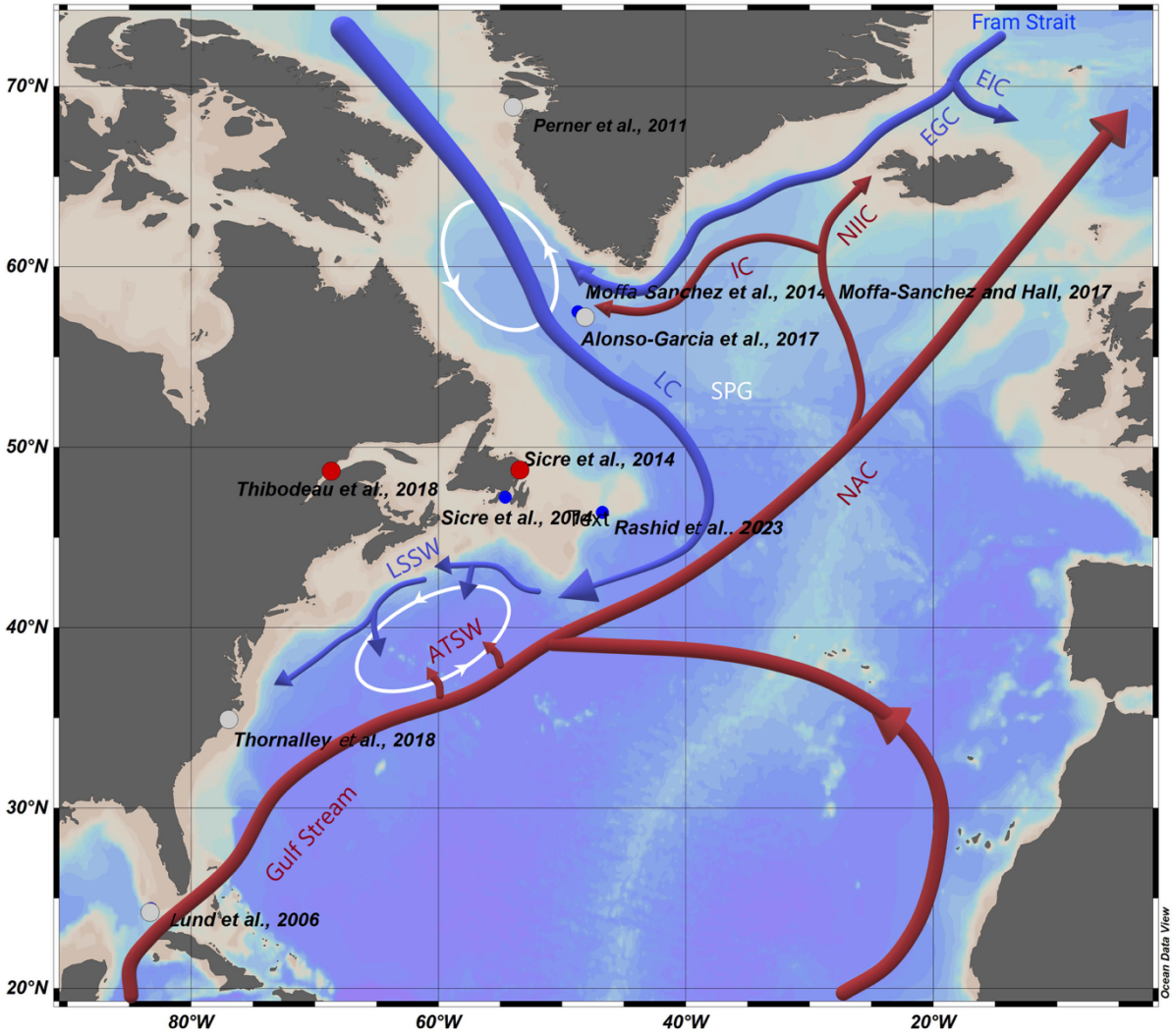

Figure 1. Map of the North Atlantic, ocean currents and locations of study cores listed in Table 1. Red dots refer to studies indicating a warming during LIA, blue dots refer to studies indicating a cooling during LIA, and grey dots refer to studies using non-temperature-related proxies. Abbreviations on the map are: ATSW= Atlantic Temperate Slope Water; EIC= East Iceland Current; EGC= East Greenland Current; IC= Irminger Current; LC= Labrador Current; LSSW: Labrador Sea Slope Water; NAC= North Atlantic Current; NIIC= North Iceland Irminger Current; SPG= sub-polar gyre; The two white circles indicate convection; the upper one refers to Labrador Sea Convection while the lower one refers to Northern Recirculation Gyre.

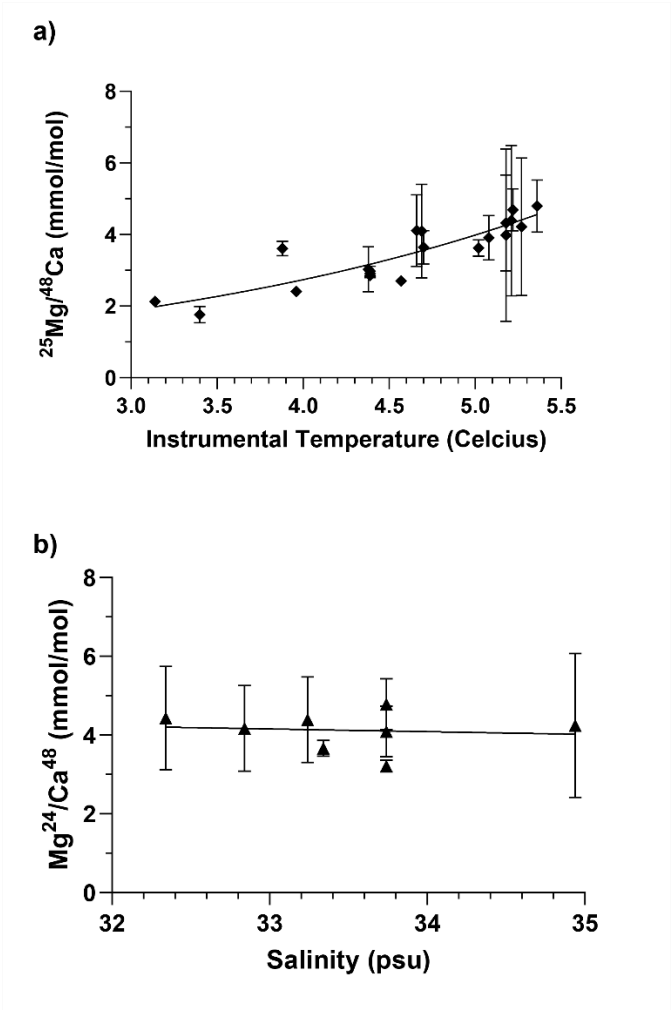

Figure 2. Best-fit curve for the MeRC-corrected 24Mg/48Ca data against a) instrumental temperature and b) instrumental salinity, respectively. Error bars were indicated as standard deviations.

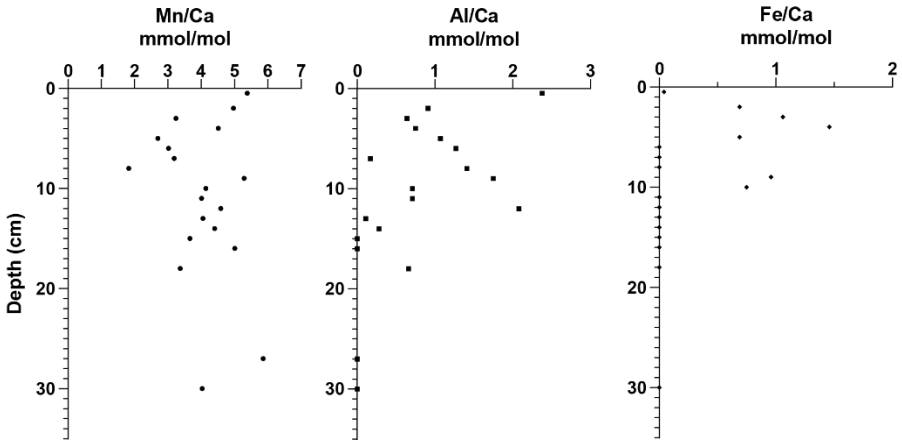

Figure 3. Ratio of contaminant (Mn, Al and Fe) on Ca downcore of CR02-23

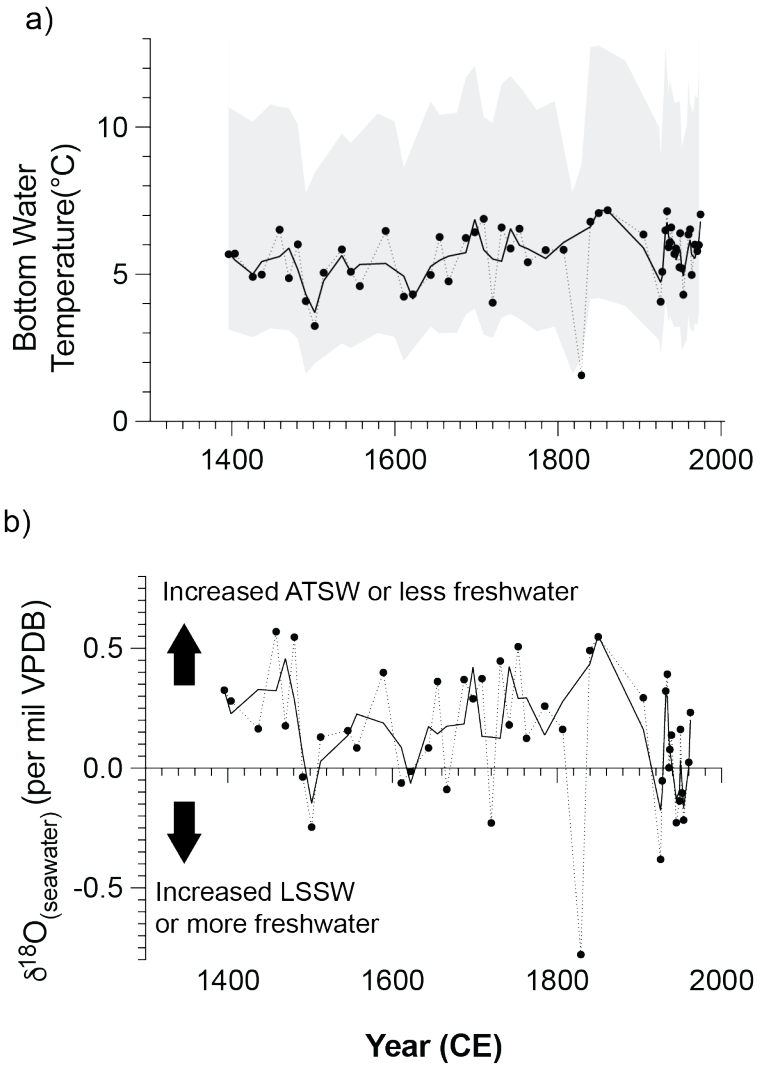

Figure 4. a) Bottom Water Temperature Reconstruction and b) seawater oxygen isotope reconstruction of the St. Lawrence Estuary from 1396 to 1975 CE. The thick lines correspond to a 3-point moving average. Temperature uncertainty was set at 95% of the confidence interval of the equation fit of the 3-point moving average, excluding the outlier at 1829 CE.

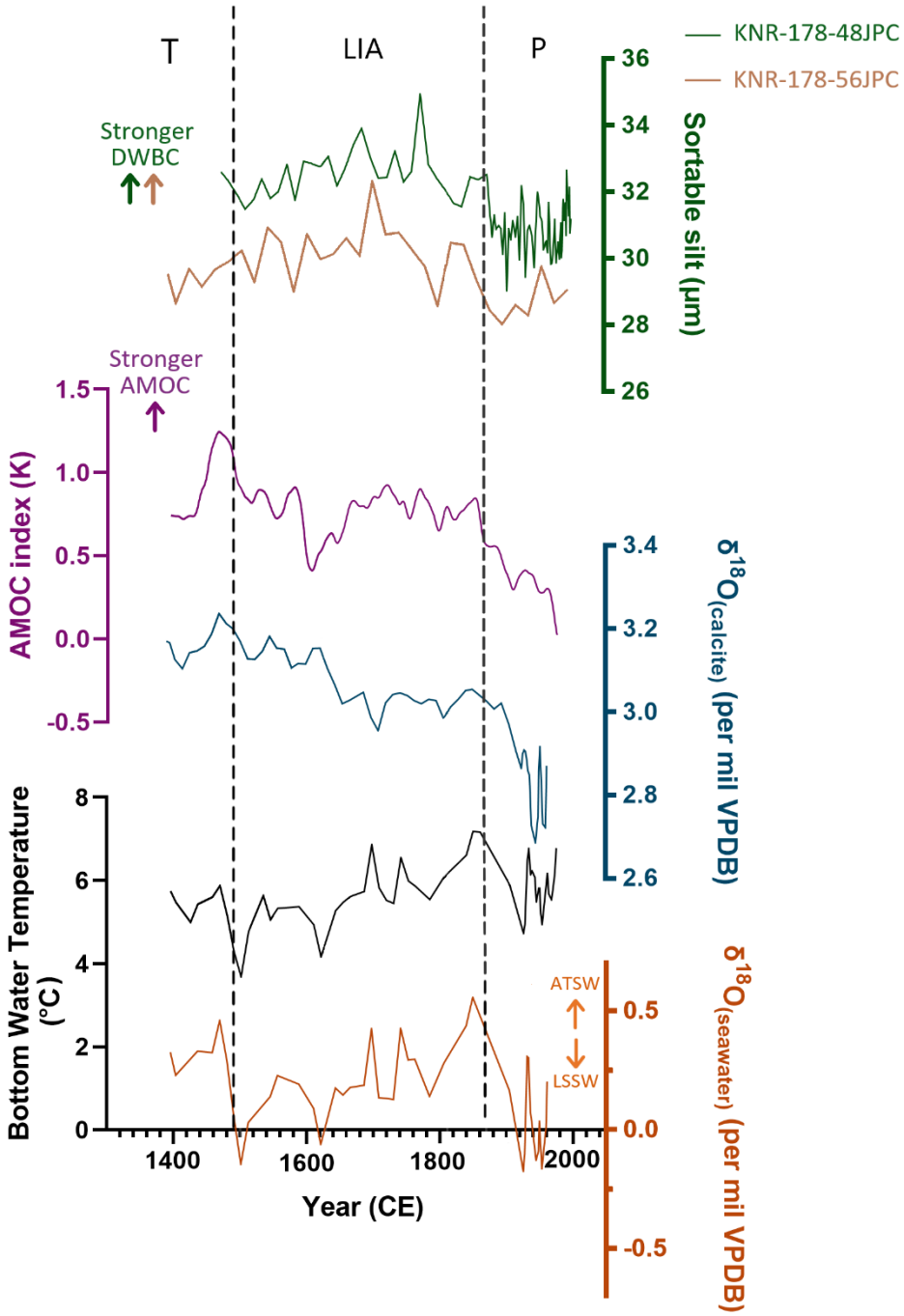

Figure 5 Comparison of selected LIA records with our result. Green (KNR-178-48JPC) and brown (KNR-178-56JPC): Sortable silt as a proxy of flow speed of deep western boundary current (Thornalley et al., 2018); Purple: smoothened AMOC index (second degree smoothening, 25 neighbours on each side; Rahmstorf et al. 2015); Dark blue: $\delta^{18}O$ of *G. auriculata* in core MD99-2220 (Thibodeau et al., 2018); Black: Bottom water reconstruction from core MD99-2220 (this study); Orange: Seawater $\delta^{18}O$ reconstruction (this study). The black vertical dashed lines indicate the suggested separation between different time intervals. T = Transition; LIA= Little Ice Age; P= Post-LIA.

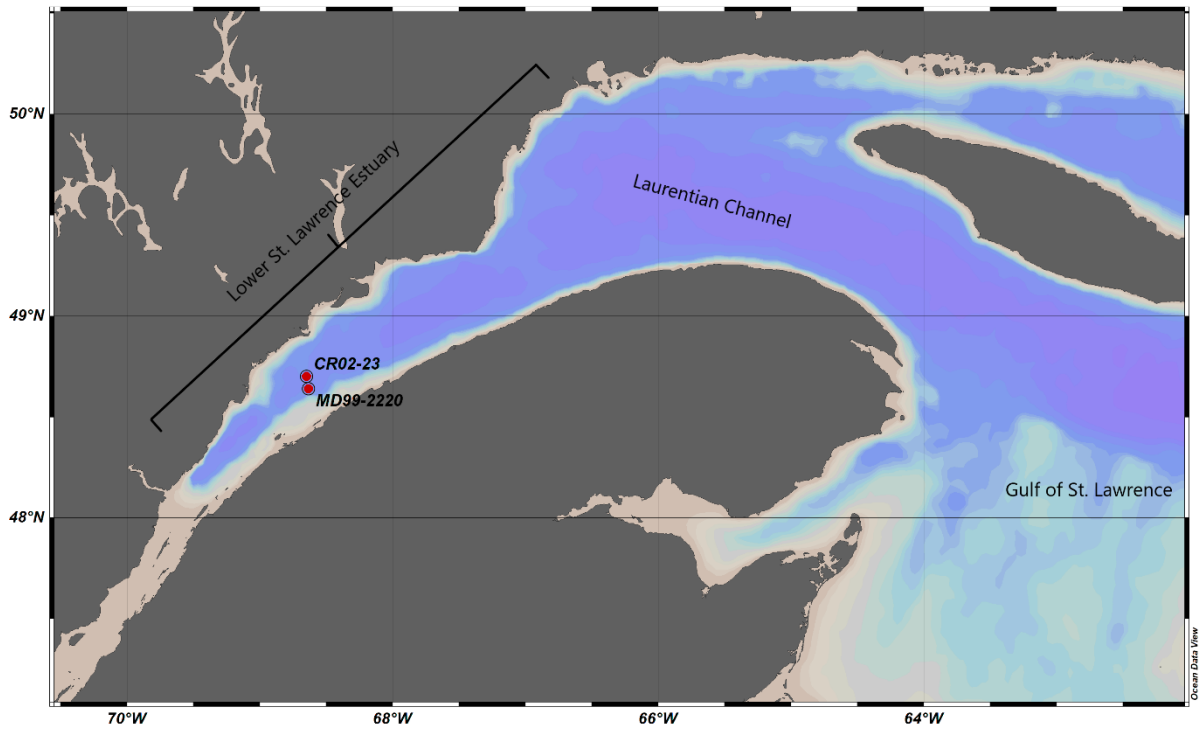

Supplementary Figure 1 Map of the St. Lawrence Estuary. Red dots indicate the location of the study cores (MD99-2220 and CR02-23).

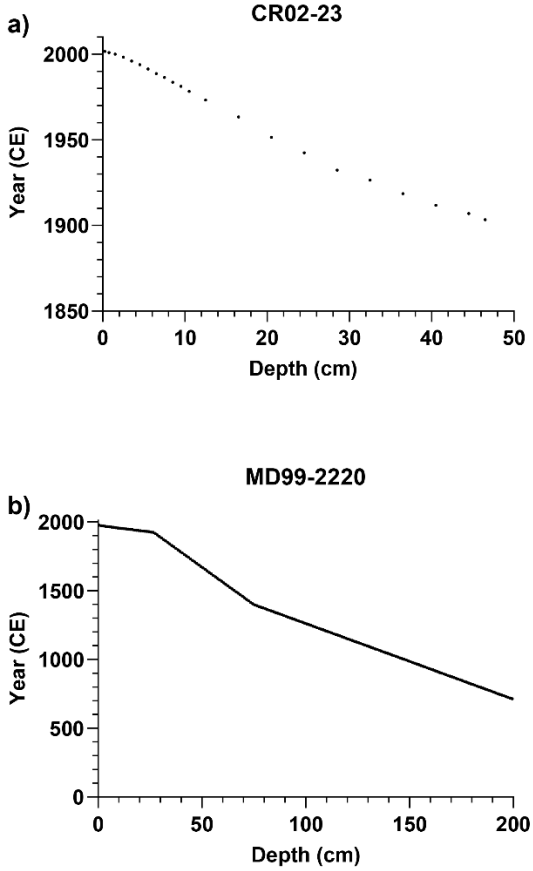

737

738 Supplementary Figure 2. Age Models of CR02-23 and MD99-2220 adopted from Thibodeau et al.
739 2010

740

741

742 Table 1 Summary of previous marine sediment proxy studies regarding oceanographic

743 changes in NW Atlantic during the LIA.

Ocean Layer	Study	Core	Proxy	Result	Oceanographic Interpretation	Timing
Sea ice	Alonso-Garcia et al. 2017	GS06-144-03	Ice-drafted debris	More ice-rafting events before the onset and during LIA	Cooling in LIA caused by previous Arctic freshwater discharges to the Labrador Sea in MCA	Pre and during LIA; ~1000–1100, ~1150–1250, ~1400–1450, ~1650–1700, ~1750–1800 CE
Near surface	Moffa-Sánchez et al. 2014	RAPiD-35-COM	δ18O; Mg/Ca; foraminifera assemblage	Lower SST of the eastern Labrador Sea; higher abundance of N. pachyderma	Increased influence of Polar Water; decreased influence of Atlantic Water in the Labrador Sea	During LIA; ~1400–1900 CE
Surface	Sicre et al. 2014	AI07-04BC, AI07-03G, AI07-11BC, AI07-12G	δ18O; Alkenone	Warmer SST along NE Newfoundland	Reduction of Labrador Sea convection; Labrador Current weakening; less freshwater contribution to Labrador Current	~1350 CE–present
Surface	Perner et al. 2011	MSM343310	Benthic foraminifera assemblage	Increasing influence of polar waters into West Greenland Current	(Atmospheric interpretation) NAO- condition during LIA	Starting in 1050 CE; highest influence at ~1650 CE
Near surface	Rashid et al. 2023	MO2009061-0217	TEX86	Abrupt cooling at ~1350 CE; warming at ~1400 CE; cooling at ~1450 CE	Warming induced by reduction in subpolar gyre and Labrador Sea; cooling induced by	~1350–1750 CE

Ocean Layer	Study	Core	Proxy	Result	Oceanographic Interpretation	Timing
					increasing polar water influence	
Near-bottom	Rashid et al. 2023	MO2009061-0217	Sortable silt	Flow rate of Labrador Current was faster in LIA	Labrador Current more vigorous in LIA; increasing rate from ~1400–1600 CE and ~1640–1700 CE	~1400–1700 CE (peaks as noted)
Near bottom	Moffa-Sánchez & Hall 2017	RAPiD-35-COM; RAPiD-21-COM	Foraminifera assemblage; sortable silt	More polar water entering Labrador Sea; reduced Labrador Sea Water in Iceland Basin	Reducing subpolar gyre strength	During LIA; ~1400–1900 CE
Near bottom	Thornalley et al. 2018	48JPC, 56JPC	Sortable silt	A decrease in flow speed of the deep western boundary current	Weakened Labrador Sea convection and AMOC at the end of LIA	At the end of LIA; after 1850 CE
Bottom water	Thibodeau et al. 2018	MD99-2220	Benthic δ18O	Lower oxygen isotope signal	More contribution to St. Lawrence Estuary from Labrador Current during LIA	Mid to end of LIA; ~1600–1900 CE
Whole water column	Lund, Lynch-Stieglitz, & Curry 2006	50MC-E; 49GGC; 16MC-A; 3MC-H; W167-79GGC; 62MC-A; 11MC-D	Planktic and benthic δ18O	Lower density gradient and vertical current shear of the Gulf Stream	Weaker Gulf Stream during LIA	Pre and during LIA; ~1200–1850 CE

744

745 Table S2 Elimination threshold for data elimination in ICP-MS.

Ratio or concentration	Threshold (mmol/mol or ppb)
Al/Ca	5.5
Mn/Ca	6
Ca	500 ppb
Mg/Ca	10
Fe/Ca	5

746

747 Table S3 Average and standard deviation of Mg/Ca ratio in each depth of core CR23-23 after
748 MeRC correction with the corresponding instrumental temperature described in Thibodeau et
749 al., 2018. NA (not applicable) refers to average with only one measurement left in the depth
750 and unavailable data for salinity. Values (except depth) were corrected to two decimal places.

Depth (cm)	$^{24}Mg/^{48}Ca$ (mmol/mol)		Instrumental Temperature (°C) (Thibodeau et al., 2018)	Instrumental salinity (psu) (Galbraith et al., 2018)
	Average	Standard Deviation		
0.5-1	4.78	0.65	5.22	33.74
2-3	3.66	0.20	5.02	33.34
3-4	4.17	1.09	4.69	32.84
4-5	3.78	0.30	4.7	NA
5-6	4.43	1.31	5.18	32.34
6-7	4.24	1.83	5.27	34.94
7-8	4.65	2.08	5.21	NA
8-9	4.17	2.39	5.18	NA
9-10	5.03	0.83	5.36	NA
10-11	4.09	0.64	5.08	33.74
11-12	4.39	1.09	4.66	33.24
12-13	3.21	0.15	4.39	33.74
13-14	3.65	0.17	3.88	NA
14-15	2.51	NA	3.96	NA
15-16	2.91	0.04	4.39	NA
16-17	2.62	NA	4.57	NA
18-19	3.05	0.81	4.38	NA
27-28	2.25	NA	3.14	NA
30-31	1.87	0.15	3.4	NA

751

752 Table S4 Comparison of best-fit curve on $^{24}Mg/^{48}Ca$ after MeRC correction. Standard errors
753 are used as errors of the linear equations *(Bryan and Marchitto, 2008)*; 95% confidence
754 interval was used as errors for the exponential equations *(Lea et al., 1999)*. p-values were
755 calculated as the 95% confidence interval. t= bottom water temperature in °C. Values in
756 equations are corrected to 4 significant figures.

	$^{24}Mg/^{48}Ca$ (mmol/mol)
Best-fit Equation (Exponential)	$Mg/Ca = 0.6341e^{(0.3740t)}$
Range of equation in 95% CI profile	Maximum: $Mg/Ca = 1.114e^{(0.5008t)}$ Minimum: $Mg/Ca = 0.3399\ e^{(0.2574t)}$
R-square	0.76
Degrees of Freedom	19
Percentage of Mg/Ca increase per 1°C increase	45.35%
Linear Equation	$Mg/Ca = (1.217 \pm 0.1746)t - (1.959 \pm 0.8132)$
R-square	0.74
p-value	<0.0001 (significant)
Mg/Ca increase per 1°C increase	1.22 mmol/mol

757

Table S5. Linear and Exponential fit correlating 300 m deep water salinity data (Galbraith et al., 2018) and two treatments of $^{24}Mg/^{48}Ca$ data. The "s" in equation represents 300m bottom water salinity. P-value was calculated with a 95% confidence interval. Standard error was used as the uncertainty of the linear equation. "NA" = not applicable. t represents water temperature in Celsius.

Linear Fit	$^{24}Mg/^{48}Ca$ (mmol/mol) vs salinity	Difference between $^{24}Mg/^{48}Ca$ (mmol/mol) and back-calculated Mg/Ca (mmol/mol) from Weldeab, Arce, and Kasten 2016 against salinity (psu)
Equation	$Mg/Ca = (-0.06881 \pm 0.2578)s - (6.426 \pm 8.635)$	$Mg/Ca = (-0.1049 \pm 0.2229)s + (3.634 \pm 7.467)$
R-square	0.01	0.04
p-value	0.80 (not significant)	0.65 (not significant)
Exponential Fit		
Equation	$Mg/Ca = 7.411e^{(-0.01752t)}$	Data too unstable for calculation
Range of equation in 95% CI profile	Maximum: $Mg/Ca = 1653e^{(0.1366t))}$ Minimum: $Mg/Ca = 0.04178\, e^{(-0.1796t)}$	NA
R-square	0.01	NA
Degree of Freedom	6	6

766 Table S6 Result of Mann-Kendall trend test and Sens's slope test on year 1490-1870 CE.

767 With a 95% confidence interval.

Mann-Kendall Trend Test (Reconstructed $\delta^{18}O_{(seawater)}$)	
Time frame	1490-1870 CE 768
z-score	2.01
Sens' slope	0.016 (positive trend)
Number of samples	24
p-value	0.04 (significant)
Mann-Kendall Trend Test (Reconstructed Temperature)	
Time frame	1490-1870 CE
z-score	2.97
Sens' slope	0.097 (positive trend)
Number of samples	25
p-value	<0.01 (significant)